Applied Surface Science 549 (2021) 149263

Contents lists available at ScienceDirect

Applied Surface Science

journal homepage: www.elsevier.com/locate/apsusc

Full Length Article

Surfactant-free synthesis of size controlled platinum nanoparticles: Insights from *in situ* studies

Jonathan Quinson [a,*,1], Alexandra Dworzak [b,c,1], Søren B. Simonsen [d], Luise Theil Kuhn [d], Kirsten M.Ø. Jensen [a], Alessandro Zana [e], Mehtap Oezaslan [b,c], Jacob J.K. Kirkensgaard [f,g,*], Matthias Arenz [e,*]

[a] University of Copenhagen, Department of Chemistry, Universitetsparken 5, 2100 Copenhagen Ø, Denmark
[b] Technical University of Braunschweig, Institute of Technical Chemistry, Technical Electrocatalysis Laboratory, 38106 Braunschweig, Germany
[c] Carl von Ossietzky University of Oldenburg, Institute of Chemistry, 26111 Oldenburg, Germany
[d] Technical, University of Denmark, Department of Energy Conversion and Storage, Fysikvej Bldg. 310, DK-2800 Kgs. Lyngby, Denmark
[e] University of Bern, Department of Chemistry and Biochemistry, Freiestrasse 3, CH-3012 Bern, Switzerland
[f] University of Copenhagen, Department of Food Science, Rolighedsvej 26, 1958 Frederiksberg C, Denmark
[g] University of Copenhagen, Niels Bohr Institute, Universitetsparken 5, 2100 Copenhagen, Denmark

ARTICLE INFO

Keywords:
Nanoparticles
Platinum
Small angle X-ray scattering (SAXS)
Size control
Surfactant-free
X-ray absorption near edge structure (XANES) spectroscopy

ABSTRACT

The controlled synthesis of surfactant-free nanoparticles (NPs) remains a challenge. To develop improved and reproducible syntheses, a deeper understanding of the formation mechanism of surfactant-free NP is key. Pt NPs in particular are important catalysts for a wide range of applications. *In situ* X-ray absorption near edge structure (XANES) spectroscopy, *in situ* small angle X-ray scattering (SAXS) and transmission electron microscopy (TEM) are used to study the formation of surfactant-free Pt NPs in alkaline ethylene glycol. For the first time, different concentrations of H_2PtCl_6 (4 mM or 10 mM), different NaOH/Pt molar ratios between 0 and 20 and a wide temperature range from 30 to 140 °C are investigated. It is shown that the NaOH/Pt molar ratio influences the kinetics of the NP formation and is a key parameter to tune in order to achieve size control. At higher NaOH/Pt molar ratio the formation of Pt NPs is slower and smaller NPs are formed in a reproducible manner across various experimental conditions. This is related to the surface properties of the NPs. NPs with a diameter ca. 1 nm are easily obtained with a NaOH/Pt molar ratio of 10–20 and their formation takes place faster at higher temperatures.

1. Introduction

Careful control of nanomaterial synthesis is key to develop nanostructures with a desired set of physical and chemical properties. The study of the formation and growth of nanomaterials is therefore particularly relevant to understand and eventually tune the resulting characteristics like size, composition and/or morphology [1–3]. Ultimately, this knowledge will help to design performant nanomaterials with properties matching to the closest requirements such as high activity and stability for a given application. Wet chemical syntheses are widely implemented worldwide to obtain nanomaterials due to their simplicity and relatively good scalability [4,5]. In this approach, the formation of nanostructures occurs in a liquid phase and an important example is the synthesis of nanoparticles (NPs). The conversion of molecular metal precursors containing often a single atom of the desired element to form NPs by nucleation of more than a thousand of these atoms can be performed in various ways: using heating devices, with or without pressure, at low or high temperature, using microwave or even

* Corresponding authors at: University of Copenhagen, Department of Chemistry, Universitetsparken 5, 2100 Copenhagen Ø, Denmark (J. Quinson). University of Copenhagen, Department of Food Science, Rolighedsvej 26, 1958 Frederiksberg C, Denmark (J.J.K. Kirkensgaard). University of Bern, Department of Chemistry and Biochemistry, Freiestrasse 3, CH-3012 Bern, Switzerland (M. Arenz).

E-mail addresses: jonathan.quinson@chem.ku.dk (J. Quinson), a.dworzak@tu-braunschweig.de (A. Dworzak), sobrs@dtu.dk (S.B. Simonsen), luku@dtu.dk (L. Theil Kuhn), kirsten@chem.ku.dk (K.M.Ø. Jensen), zanaeles@yahoo.it (A. Zana), m.oezaslan@tu-braunschweig.de (M. Oezaslan), jjkk@food.ku.dk (J.J.K. Kirkensgaard), matthias.arenz@dcb.unibe.ch (M. Arenz).

[1] These authors equally contributed to the work.

https://doi.org/10.1016/j.apsusc.2021.149263
Received 8 October 2020; Received in revised form 4 February 2021; Accepted 5 February 2021
Available online 11 February 2021
0169-4332/© 2021 The Authors. Published by Elsevier B.V. This is an open access article under the CC BY-NC-ND license (http://creativecommons.org/licenses/by-nc-nd/4.0/).

UV light [6–8]. The freedom to tune various experimental parameters gives opportunities to control the nanomaterial properties. This makes wet-chemical syntheses, and especially colloidal syntheses, ideal to study and optimize the production of nanomaterials for various applications [9]. Nevertheless, a clearer understanding of the driving force of nanomaterial formation is of prime importance and much needed [10]. The synthesis of nanomaterials is still mostly driven by the skills of experimentalists by trials and errors which are often difficult to rationalize. The synthesis of nanomaterials is then still often referred to as 'black art' [10–12].

To advance our understanding of NP formation, a recent focus is on *in situ* studies where information is gathered *as* the materials form [13–17]. The benefits of *in situ* studies are to gain real time information on the evolution of nanostructures from the molecular species in colloidal syntheses. It is commonly agreed that the general formation pathway of NPs proceeds by a nucleation followed by growth mechanism(s) [10,18]. With *in situ* studies, the specific influence of different parameters during nucleation and/or growth can be rationalized to eventually propose improved synthesis strategies [14,15,19–21]. In particular, controlling the size of precious metal NPs is important due to the limited supply of these resources. Precious metals are key catalysts in a range of application, e.g. for chemical conversion, but also in various energy conversion devices like fuels cells and electrolysers [22–24], and intensely studied for their size-dependent optical properties. Furthermore, precious metals are increasingly considered in the medical sciences [25,26]. Specifically, it is important to control the size of platinum (Pt) NPs because size determines catalytic activity, available surface area for electrocatalysis and stability to a great extent [27].

A major drawback in most colloidal syntheses is the need for additives [4,28]. Additives like polymers or surfactants present on the NP surface are used to prevent NP agglomeration, sintering and to control size. However, these additives typically need to be removed after NP formation; especially in catalysis where a fully accessible precious metal NP surface is highly desired. Removal of surfactants requires time and energy intensive steps, often hazardous chemicals, and add the risk of altering the structure of the as-prepared catalysts [29,30]. In that respect, surfactant-free syntheses present valuable features. It has been established since 2000 that in the polyol process, where alkaline ethylene glycol is used as solvent and reducing agent, the reduction of various precious metal precursors leads to small NPs without the need for surfactants [31,32]. The NPs are protected against agglomeration and sintering by CO groups adsorbed on the surface and electrostatic repulsion [33]. This approach has been successfully applied to develop performant catalysts [34,35]. Despite the facility of this method, an abundant literature still stresses the need for surfactants in colloidal synthesis [4,28]. Despite the multiple advantages of surfactant-free approaches [5,22], the understanding of surfactant-free colloidal syntheses needs to be improved and their use advertised.

In order to achieve a reliable size control in the surfactant-free polyol synthesis, we have recently reported that in contrast to a common statement, it was not the 'pH' that controls the size of Pt NPs obtained from H_2PtCl_6 in the surfactant-free polyol synthesis, but rather the molar ratio of base (NaOH) to metal precursor [35]. To confirm and investigate further this phenomenon, *in situ* X-ray absorption spectroscopy (XAS) and small angle X-ray scattering (SAXS) studies together with transmission electron microscope characterization (TEM) are here reported to rationally guide the development of more robust syntheses of size controlled surfactant-free Pt NPs. For the first time, the NP formation is investigated *in situ* across a range of precursor concentration (4 mM and 10 mM), NaOH/Pt molar ratios of 0, 2.25, 4.50, 10 and 20 and a wide temperature range from 30 to 140 °C.

2. Material and methods

Chemicals. All chemicals were used as received: $H_2PtCl_6{\cdot}6H_2O$ (99.9% Alfa Aesar); NaOH (98%, Alfa Aesar); ethylene glycol (99+%, Sigma-Aldrich), ethanol (VWR, absolute, ≥ 99.5%).

Synthesis of Pt NPs. The synthesis of the Pt NPs is further detailed below for the specific case of *in situ* XANES and *in situ* SAXS. In short, the synthesis follows the general recipe developed by Wang *et al.* in their seminal work [31] and further developed along the years [34,35]. Alkaline (NaOH) ethylene glycol plays the role of solvent, stabilizing and reducing agent for H_2PtCl_6 reduction. Upon heat treatment, surfactant-free 'unprotected' NP are formed, i.e. mainly protected by CO groups adsorbed on the NP surface [33].

Transmission electron microscopy (TEM). TEM micrographs were acquired on samples collected after *in situ* SAXS experiments and stored in a fridge prior to sample preparation for TEM analysis, diluted with ethanol and dropped on carbon coated nickel TEM grids (Quantifoil). A JEOL 2100 TEM operated at 200 kV was used for imaging. Particle size and morphology were estimated by recording images at least three at different magnifications (x300 000, x400 000, x500 000) in minimum three randomly selected areas.

***In situ* X-ray absorption near edge structure (XANES) spectroscopy.** XANES measurements were carried out at the SuperXAS beamline of the Swiss Light Source (SLS), Switzerland with a beam current of around 400 mA and a storage ring energy of 2.4 GeV. The acquisition of the Pt L_3 edge (11 564 eV) XANES spectra was performed in transmission mode by using N_2-filled ionization chambers with lengths of 15 and 30 cm for the incident (I_0) and transmitted (I_1 and I_2) X-ray intensities, respectively. The averaged spectra were analyzed by using the IFEFFIT software suite [36]. All spectra were background subtracted and normalized. The energy units (eV) were converted to photoelectron wave vector k units ($Å^{-1}$) by assigning the photoelectron energy origin, E_0, corresponding to $k = 0$, to the first inflection point of the absorption edge.

Linear combination fit (LCF) method was carried out to establish the oxidation state of Pt species in the colloidal dispersions by using the respective XANES reference spectra of K_2PtCl_4 in ethylene glycol, K_2PtCl_6 in ethanol and Pt foil. An example of LCF is reported in Fig. 1. See **Figure S1** for further examples of data fits. The relative weight percentages of Pt^{IV}, Pt^{II} and Pt^0 species and the related parameters such as white line intensity, shift of energy (ΔE_0) at the corresponding edge and R factor (closeness of the fit as quality parameter, defined as the ratio between the sum of the square of the difference between data and fit and the sum of the square of the data, for the data points in the fitting region: the smaller the R factor, the better the fit from a statistics point of view) were determined using LCF analysis. The LCF was obtained as

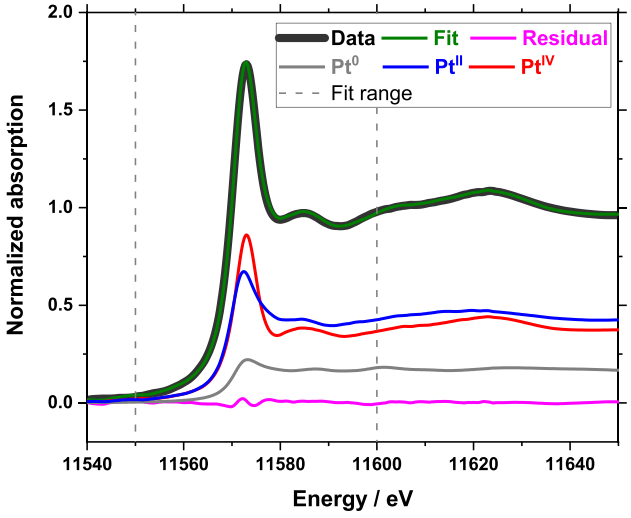

Fig. 1. Example of XANES data fit and LCF analysis for 4 mM H_2PtCl_6 with NaOH/Pt molar ratio of 2.25 after 392 s of exposure to the X-ray beam showing the relative contribution of Pt^{IV}, Pt^{II} and Pt^0 to the fit.

normalized μ(E) fit with following parameters: Range of fit was between −20 eV and +30 eV relative to E_0, the components were forced to be between 0 and 1 and to sum up to 1. An overall E_0 shift was used. The samples with a 4 mM H_2PtCl_6 concentration were placed in Nalgen vials. All experiments were performed at room temperature.

***In situ* small angle X-ray scattering (SAXS).** The size of the nanoparticles obtained was assessed by SAXS measurements using a SAXSLab instrument (JJ-XRay) with a Rigaku 100 XL + micro focus sealed X-ray producing a photon beam with a wavelength of 1.54 Å tube and a Dectris 2D 300 K Pilatus detector installed at the Niels Bohr Institute of the University of Copenhagen. To follow *in situ* the formation of the NPs, two different concentrations of H_2PtCl_6 were used: 4 mM and 10 mM. Different NaOH/Pt molar ratios were studied: 0, 2.25, 4.50, 10 and 20. The temperature range investigated was between 30 °C and 140 °C, with a more detailed focus between 95 °C and 110 °C. The reaction mixture were placed in sealed quartz capillaries (10 μm wall thickness, 1 mm diameter, 8 cm long, Hildenberg) placed in the same temperature control holder heated up at 10 °C min^{-1} to the desired temperature. In the interest of time, the experiments were stopped when the intensity measured by SAXS was constant over time. A constant signal was considered an indication that the system had reached an equilibrium state in terms of number and size of NPs formed. The focus is therefore here on the kinetics of nucleation as it is shown that their further growth is very slow and moderate, in agreement with previous reports [32]. The first recorded SAXS spectrum at room temperature was used as background. The data recorded with an acquisition time of 5 min were then background subtracted before fitting. An example of data set and related fits is given in Fig. 2. Further data set and fits are available in the *Supplementary Information*.

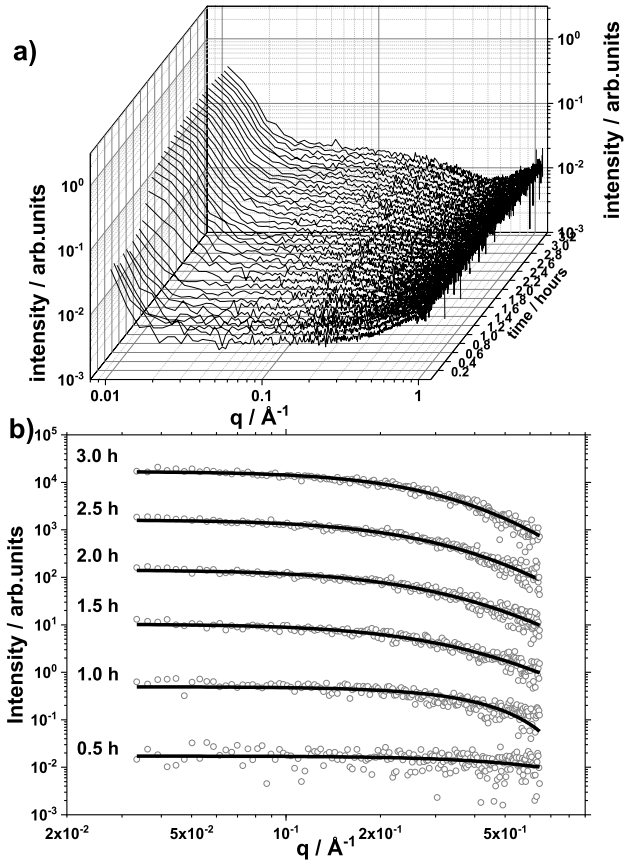

Fig. 2. Example of (a) SAXS data as measured and (b) SAXS data after background subtraction (circles) and related fits (solid line) for different times as indicated. The experiment was conducted with 10 mM H_2PtCl_6 with a NaOH/Pt molar ratio of 20 at 110 °C.

For data reduction the SAXGUI software was used, the two-dimensional scattering data were azimuthally averaged, normalized by the incident radiation intensity, the sample exposure time and the transmission. They were further corrected for background and detector inhomogeneities. The radially averaged intensity I(q) is given as a function of the scattering vector $q = 4\pi\cdot\sin(\theta)/\lambda$, where λ is the wavelength and 2θ is the scattering angle. The background corrected scattering data was fitted by a power law (to take into account the behavior at low q) and a polydisperse spheres model described by a volume-weighted log-normal distribution [37]. The scattering data are fitted to the following expression:

$$I(q) = A.q^{-n} + C\cdot\int P_s(q,R)\ V(R)D(R)dR$$

where $A\cdot q^{-n}$ corresponds to the power law where A and n are free parameters; C is a scaling constant, P_s the sphere form factor, V the particle volumes and D(R) the log-normal size distribution. The sphere form factor is given by:

$$P_s(q,R) = \left(3\frac{sin(qR) - qRcos(qR)}{(qR)^3}\right)^2$$

and the log-normal distribution by:

$$D(R) = \frac{1}{R\sigma\sqrt{2\pi}}\exp\left(\frac{-\left[\ln\left(\frac{R}{R_0}\right)\right]^2}{2\sigma^2}\right)$$

where σ is the variance and R_0 the geometric mean of the log-normal distribution. The fitting was done using home written MATLAB code to optimize agreement between data and model. The free parameters in the model are: A, n, R,σ, and C. R was evaluated in Å and the diameter of the NP was evaluated in nm as$0.2e^{(ln(R)+\frac{\sigma^2}{2})} \pm 0.2\sqrt{(e^{\sigma^2}-1)e^{(2\ln(R)+\sigma^2)}}$.

3. Results and discussion

3.1. *In situ* XANES

In order to provide insight into the effect of different NaOH/Pt molar ratios on the formation kinetics of Pt NPs, *in situ* XANES studies were first performed. Conveniently, the beam induces a nucleation and thus the formation of the NPs did not require an advanced set up. By simply exposing the reaction solution to the X-ray beam, a clear darker line is observed in the solution containing the precursor in few seconds to minutes. This darker line follows the direction and axis of the incident beam and is attributed to the formation of colloidal NPs. This is confirmed by evaluating the relative ratios of Pt species in different oxidation states by LCF analysis of the XANES data. The changes in the relative quantities of Pt^{IV}, Pt^{II} and Pt^0 as a function of time of exposure to the beam for a concentration of 4 mM H_2PtCl_6 and NaOH/Pt ratios of 2.25, 4.50, 10 and 20, are shown in Fig. 3. Without adding NaOH and for the time of exposure considered here, no metallic NPs (Pt^0) are formed.

A clear trend observed for all samples is the decrease in the Pt^{IV} species while Pt^{II} species form over time and only later Pt^0 is generated e.g. as shown in Fig. 3**d**. These results are in agreement with the generally assumed reduction mechanism of Pt precursors to form metallic NPs. Although the detailed mechanism of reduction of Pt precursors to NPs is still debated [3,7,13,14,19,38], the general pathway is considered to be as follow: first, the Pt^{IV} species are converted to Pt^{II}. This corresponds to an induction phase during synthesis with almost no noticeable change in the color of the solutions. After this induction period, the formation of darker spot in the solution suggests that nucleation occurs and this corresponds to the reduction of the Pt^{II} species to Pt^0, followed by a growth of NPs (Pt^0). This general trend is

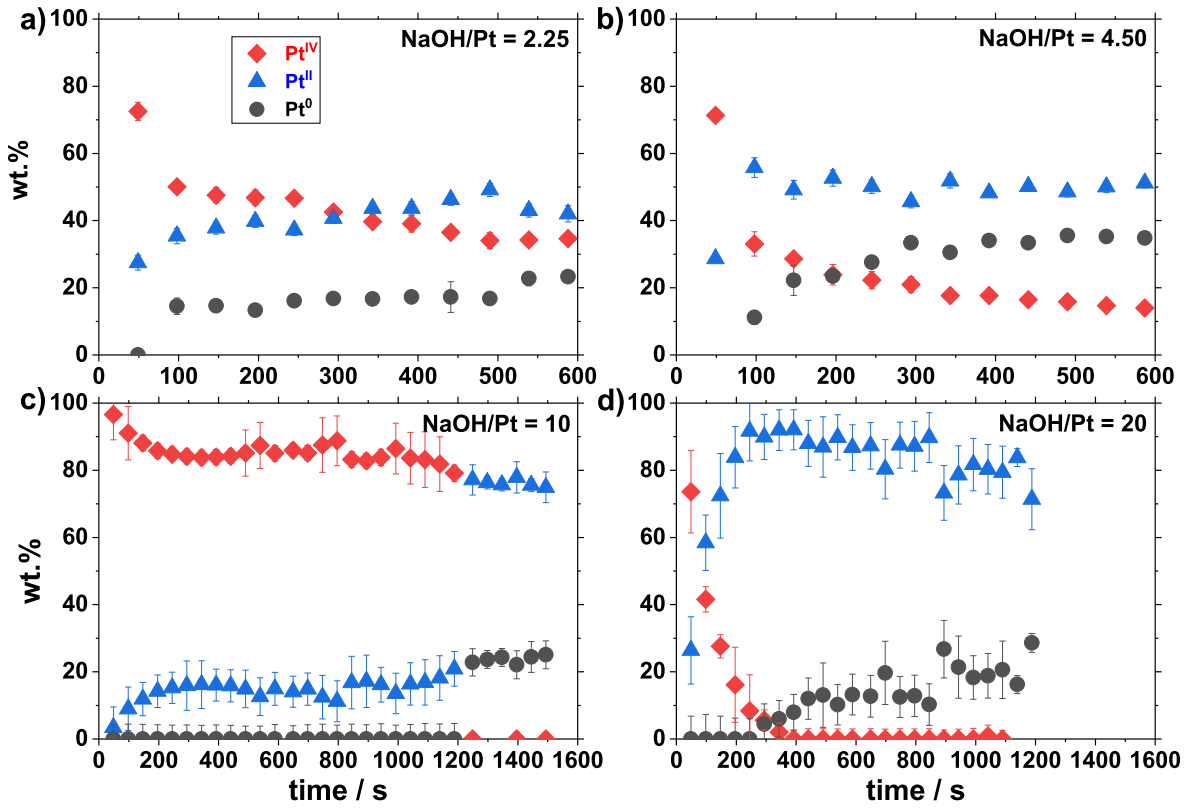

Fig. 3. LCF analysis of the XANES data for beam induced reduction of 4 mM H_2PtCl_6 with different NaOH/Pt molar ratios of (a) 2.25, (b) 4.50, (c) 10 and (d) 20 in alkaline ethylene glycol. Every data point has error bars, but some are too small to be seen on the plot.

especially clear in Fig. 3**d**. Another trend from this set of data is that the time needed to form Pt NPs, e.g. defined as an amount of Pt^0 species > 15 wt%, increases as the NaOH/Pt molar ratio increases. For lower NaOH/Pt molar ratio, e.g. of 2.25, some Pt^0 is detected after only 100 s after exposure to the beam whereas it takes up to 300 s for higher NaOH/Pt ratio, e.g. 20. The results show that a higher NaOH concentration leads to a longer time to observe nucleation and growth of Pt NPs.

The apparent steady state and partial conversion to Pt^0 obtained (<30 wt%) in these data probably comes from the fact that the volume of solution probed by the beam was very small as compared to the total volume. Slow diffusion of the species in the viscous ethylene glycol solvent outside the volume probed by the beam can account for the limited apparent yield. In Fig. 3**c**, the sudden formation of Pt^0 is consistent with observation by eye that the reaction seems more progressive at lower and higher NaOH/Pt molar ratio and can be attributed to a burst-like formation mechanism [7,39] The experimental conditions remain relatively *uncontrolled* in this respect and the high energy of the beam can render detailed analysis challenging. In particular, the role of X-rays to induce the synthesis or to generate heat due to the high intensity provided by synchrotron beams, is not clear. Several reports using different Pt syntheses do not stress what happens at room condition without incentive to initiate the reaction [15,40]. Thus, we want to emphasize that if the opportunity to use beam-induced synthesis is here exploited, the results, however, need to be considered with care and may not be fully representative of what is happening when the synthesis if thermally induced. Nevertheless, these experiments give a general understanding of the reduction steps of the Pt precursor.

3.2. *In situ* SAXS measurements

To further relate the kinetics of NP formation observed to size control, *in situ* SAXS measurements were performed. SAXS measurements make it possible to retrieve the size of the NPs after analysis of the scattering patterns obtained under exposure to X-rays [37]. Several parameters e.g. Pt precursor concentration, NaOH/Pt ratio and temperature were considered for this study. The concentration of H_2PtCl_6 was 4 mM or 10 mM, while the temperature range was from 30 to 140 °C. The NaOH/Pt molar ratios were varied from 0, 2.25, 4.50, 10 to 20. The related experimental conditions and the color code used thereafter are summarized in Table 1. In contrast to previous *in situ* SAXS work [39], the present study scrutinizes for the first time several different NaOH/Pt molar ratios as well as different temperatures and different initial concentrations of H_2PtCl_6. In particular, both the Pt precursor concentration *and* the NaOH concentration are changed at the same time while their molar ratio is kept constant.

In order to discard any effect of the X-ray source used for the *in situ* SAXS experiments on the nucleation and formation of the Pt NPs, reference experiments at low temperature, see entry **A** in Table 1, and *relatively* low temperature, e.g. 85 °C see entry **B** in Table 1, were performed. For a set of experiments performed at 30 °C, no NP formation could be probed even after more than 8 h of exposure to X-rays, see **Figure S2-S3**. This difference with the XANES data can be inferred to the much lower intensity of the laboratory source compared to a synchrotron beam. In the case of the experiment performed at 85 °C, a small increase of the NP diameter is observed over time, but it takes more than 5 h to record a significant increase and evaluate a diameter larger than 0.5 nm, see **Figure S4**. It is therefore concluded that the X-ray source used here has a minor influence on the NP formation in agreement with previous report [39]. The surfactant-free synthesis of Pt NPs in alkaline ethylene glycol is reported to best proceed above 100 °C and typically is carried out at around 160 °C [32] The results obtained here at 85 °C confirm this statement.

It is commonly agreed that without NaOH, no NPs are formed [4,31]. Our results also confirm this statement. In the experiments carried out without NaOH, see entries **C** or **H** in Table 1, either no reaction seems to happen (e.g. at lower temperature and low concentration) or a black

Table 1
Overview of samples and experimental parameters for *in situ* SAXS. The mean sizes reported correspond to the end of the experiment.

Entry	H_2PtCl_6 [mM]	NaOH [mM]	NaOH/Pt	T [°C]	Time [h]	Symbol	Mean size [nm]
A	10	45	4.50	30	8.7	▲	–
B	4	80	20	85	10.7	★	0.7 ± 0.3
C	10	0	0	125	8.0	●	–
D	4	9	2.25	95	1.5	▲	3.9 ± 0.2
E	4	18	4.50	95	1.2	■	2.6 ± 0.8
F	4	40	10	95	1.4	⬟	0.7 ± 0.3
G	4	80	20	95	4.0	★	0.8 ± 0.3
H	4	0	0	110	2.6	●	–
I	4	9	2.25	110	2.9	▲	2.4 ± 0.8
J	4	18	4.5	110	3.0	■	2.5 ± 0.8
K	4	40	10	110	5.4	⬟	0.6 ± 0.3
L	4	80	20	110	2.1	★	0.7 ± 0.3
M	10	22.5	2.25	95	2.5	▲	4.7 ± 0.1
N	10	45	4.50	95	1.9	■	2.6 ± 0.7
O	10	100	10	95	4.1	⬟	1.0 ± 0.3
P	10	200	20	95	4.2	★	0.7 ± 0.4
Q	10	22.5	2.25	110	1.1	▲	3.3 ± 0.4
R	10	45	4.50	110	1.1	■	2.3 ± 0.5
S	10	100	10	110	2.4	⬟	1.0 ± 0.4
T	10	200	20	110	3.3	★	1.0 ± 0.3
U	10	200	20	125	1.7	★	1.0 ± 1.0
V	10	200	20	140	1.8	★	0.9 ± 0.4

deposition is observed but no colloidal dispersions are obtained (higher temperature and higher concentration), see **Figure S2, S5**.

Several experiments were then performed at 95° C and 110 °C. These temperatures are relatively low for the polyol synthesis, which is typically performed above 150 °C [32]. These values were chosen to slow down NP formation kinetics to investigate the effect of other parameters like H_2PtCl_6 concentration and NaOH/Pt molar ratio. For a concentration of 4 mM H_2PtCl_6 and NaOH/Pt molar ratio of 2.25, no reaction seems to occur at 95 °C, whereas at 110 °C a dark film is formed that covers the inner wall of the capillaries, indicating the reduction of the soluble Pt species to more bulk-like platinum, see **Figure S6**. In both cases, no colloidal dispersions are obtained (see entries **D** and **I** in Table 1). For the other NaOH/Pt molar ratios of 4.50, 10 and 20, colloidal dispersions are obtained (see entries **E**, **F**, **G** and **J**, **K**, **L** in

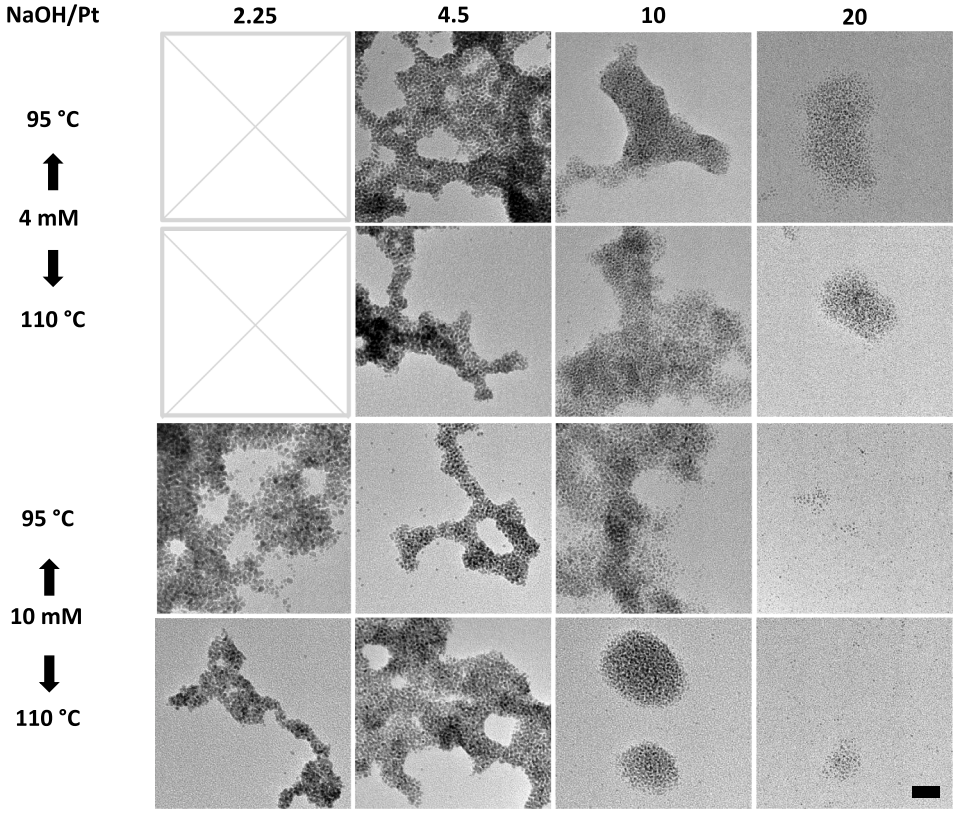

Fig. 4. TEM micrographs of the surfactant-free Pt NPs obtained under different experimental conditions: H_2PtCl_6 concentration, temperature and NaOH/Pt molar ratio, as indicated. All micrographs were recorded at the same magnification and the scale bar is 20 nm. Pictures of the related solutions colloidal dispersions are displayed in Figure S6.

Table 1). For a concentration of 10 mM H_2PtCl_6, colloidal dispersions are formed at NaOH/Pt molar ratios of 2.25, 4.5, 10 and 20 (see entries **M** to **T** in Table 1).

To confirm that NPs are formed and size control is achieved, TEM analysis of the samples was performed after *in situ* SAXS synthesis, see Fig. 4. A clear trend towards smaller size of formed NPs as the NaOH/Pt molar ratio increases is confirmed. It was also more challenging to find NPs on the grids corresponding to experiments performed at higher NaOH/Pt molar ratios (e.g. 20) which suggests - without being an *absolute* proof - a limited yield under these conditions. As the concentration of NaOH increases (e.g. for a given temperature and a given H_2PtCl_6 concentration) the resulting suspensions after reaction were lighter, see **Figure S6**. Since the time of synthesis was about the same for experiments conducted at NaOH/Pt molar ratio of 2.25 and 4.50, see Table 1, these results stress that indeed a certain amount, i.e. *enough,* NaOH is required for the reaction to proceed to the formation of colloids. The reactions at NaOH/Pt ratios of 10 and 20 were longer than those at lower NaOH/Pt ratio, yet the resulting solutions were lighter. This is especially marked for the set of experiments with 10 mM H_2PtCl_6 performed at 95 °C, **Figure S6**, and is in agreement with previous reports [39]. This can be explained by a lower conversion yield of H_2PtCl_6 to NPs and/or different NP size obtained under these conditions. These two hypotheses are further discussed below in light of the time dependence of the NP diameter.

3.3. Influence of NaOH/Pt ratio on nanoparticle diameter over time

To discuss the effect of the NaOH/Pt molar ratios in detail, the evolution of the NP diameter as a function of time retrieved from *in situ* SAXS experiments was studied and is illustrated in Fig. 5. The general intensity profile obtained is in line with previous reports [39]. For a period of time, data fitting is poor due to low signal-to-background ratio and extremely small NP sizes with high size deviation are retrieved. After an induction period, a clear size increase is observed while the standard deviation on the evaluated diameter retrieved from SAXS analysis is relatively small despite the absence of surfactant, in agreement with previous work [35,39].

In situ SAXS analysis confirms that as the NaOH/Pt molar ratio increases, smaller NPs are obtained. It is observed that size and general time dependency of the diameter are the same for a given NaOH/Pt ratio regardless of H_2PtCl_6 concentration, NaOH concentration or temperature. For a NaOH/Pt molar ratio of 2.25, corresponding to data points indicated with triangles in Fig. 6, after a period of ca. 1 h where the size of the NPs increases, a size decrease is observed. This can be related to a decrease in the intensity recorded, **Figure S7**, indicative of the formation of macroscopic structures like films, as evidenced from the photographs in **Figure S6** with black spots and no colloidal dispersions. This confirms that a minimum NaOH/Pt molar ratio is required to perform the synthesis and to obtain a colloidal dispersion of NPs.

For higher NaOH/Pt molar ratio, colloidal dispersions are achieved. The size obtained with a NaOH/Pt ratio of 4.5 is around 2.5 nm in all samples. For NaOH/Pt molar ratios of 10 and 20 the size obtained is about the same and around 1.0 nm. At these higher NaOH/Pt ratio, the time needed to reach a constant diameter is longer than at lower NaOH/Pt ratios, in good agreement with the XANES data discussed above in Fig. 3 as well as previous observations that too high NaOH

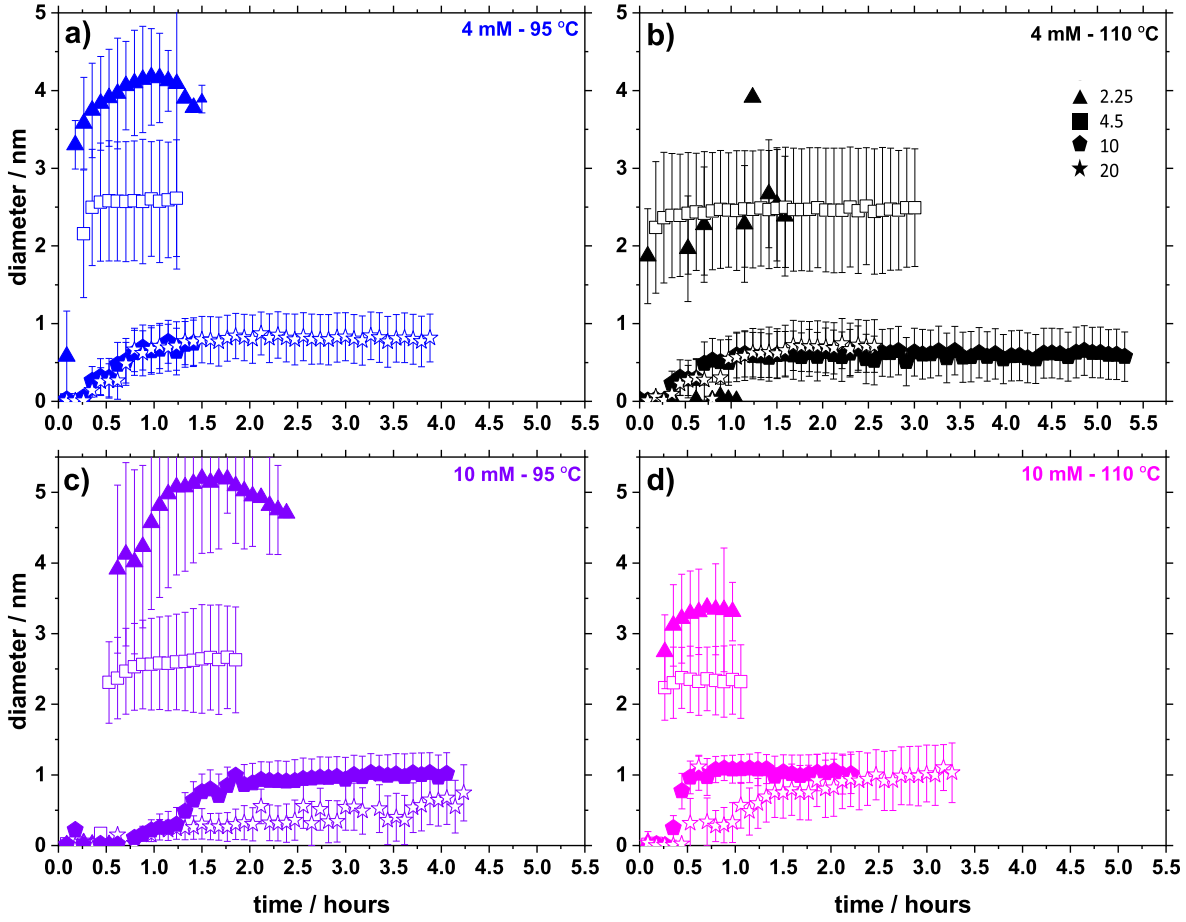

Fig. 5. NP diameter estimated by *in situ* SAXS characterisation for Pt NPs obtained using different experimental conditions: H_2PtCl_6 concentration (4 or 10 mM), temperature (95 or 110 °C) and NaOH/Pt molar ratio (2.25: triangle; 4.50: square; 10: pentagon; 20: star), as indicated. Example of the related fits can be found in Figure S8. Every data point has error bars, but some are too small to be seen on the plot.

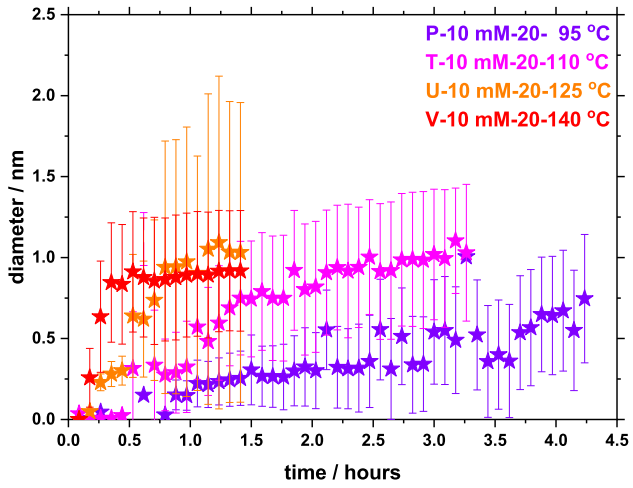

Fig. 6. NP diameter estimated from *in situ* SAXS data for Pt NPs obtained using 10 mM H_2PtCl_6 concentration, a NaOH/Pt molar ratio of 20 and temperature as indicated. For clarity, the error bars are not displayed when they were greater than 1 nm due to low signal-to-background-ratio at the beginning of the synthesis typically leading to a size estimation below 0.1 nm.

concentrations slow down the reaction when the H_2PtCl_6 concentration is fixed [39]. For a concentration of 10 mM H_2PtCl_6, it is especially clear here that for a NaOH/Pt molar ratio of 20 the growth kinetics is slower than for a NaOH/Pt ratio of 10.

These observations can be rationalized in light of the stabilization mechanism of the NPs and in particular *via* surface stabilization. It is expected that slow reduction kinetics lead to fewer seed formation and favor the growth of larger and polydispersed NPs. The formation of relatively monodispersed Pt NPs is then often described to proceed *via* a 'burst-like' phenomenon where suddenly several seeds form [41]. This type of behavior is especially clear at higher temperature, see Fig. 5 and also observed using alkaline methanol as solvent [38]. However, this model requiring a burst was recently challenged and it was described that relatively monodispersed NPs could be obtained provided that '*smaller particles grow faster than larger ones*' [42]. A possible explanation for this comes from the *ligand effect* where ligand will slow down the growth of the larger NPs [43].

A *ligand* effect may actually be found in the present case, despite the absence of surfactant. First, multiple *NaOH concentration-dependent* equilibria are expected between the various Pt complexes possibly formed such a $Pt^{IV}Cl_6^{2-}$, $Pt^{II}Cl_4^{2-}$, $Pt^{II}(OH)_4^{2-}$ and the formed NPs. This can first account for the different formation kinetics observed for different NaOH/Pt molar ratios [44]. The role of glycolate more likely formed under alkaline conditions cannot be excluded in the stabilization of smaller NPs [34]. It is also expected that CO and OH– species present on the Pt NP surface contribute to the stabilization [33,35]. In relative high amount of base, and thus higher NaOH/Pt ratio, the hydroxyl-related protection is more likely. The resulting electrostatic repulsion of the negatively charged complexes like $Pt^{II}Cl_4^{2-}$ and negatively charged NPs may limit the growth of already formed NPs by preventing further reduction of the Pt^{II} on their surface. This as well could account for the formation of smaller NPs at high NaOH/Pt molar ratio. Furthermore, it well documented that adsorbed CO (CO_{ad}) is observed on Pt NP surface in ethylene glycol [33,38,45] and the formation of CO_{ad} is relatively slow. The slower kinetics for NP formation observed for high NaOH/Pt molar ratio may favor the formation of enough CO_{ad} that stabilize the slowly growing NPs. The CO_{ad} *protection* may take place only at large enough NPs, ca. 1 nm, where enough favorable sites for CO adsorption are formed and thus *smaller particles grow faster than larger ones*. At low NaOH/Pt molar ratio the adsorption of CO may be too slow to happen compared to the fast formation of the NPs. This phenomena would explain the size around 1 nm reproducibly achieved here across various experimental conditions.

3.4. Effect of temperature

At a lower concentration of 4 mM H_2PtCl_6 and regardless of the NaOH/Pt ratio, the NP formation kinetics are very similar whether the synthesis was performed at 95 or 110 °C, see Fig. 5**a,b**. However, for 10 mM H_2PtCl_6 the formation of NPs proceeds faster at higher temperature, see Fig. 5**c, d**. Since it is established that a NaOH/Pt ratio of 20 is a suitable ratio to obtain small NPs but that this ratio could lead to slow kinetics at low temperature, the effect of temperature for these experimental conditions was further investigated (see entries **P**, **T**, **U** and **V** in Table 1). The evaluated NP diameters are displayed in Fig. 6, see also **Figure S9-S10** for the SAXS data and related fits. The size obtained for all experiment show a similar plateau always around 1.0 nm regardless of the temperature. This confirms that a high NaOH/Pt molar ratio is key to achieve reliable size control of small NPs but this size control is robustly reproduced regardless of other parameters like temperature. As the temperature increases, it takes less time to reach a stable intensity signal in the *in situ* SAXS experiments, indicative that the NPs formation has already been completed. The color of the colloidal dispersion obtained in all cases is darker, suggesting a higher yield for NP formation, despite shorter time of synthesis, see **Figure S11**. These results are in line and justify the choice to typically perform the synthesis at 150 °C or above [32].

4. Conclusions

The study presented confirms that surfactant-free syntheses are ideal model reactions to gain more insight into the formation mechanism of NPs. Rational guidelines to select experimental parameters, previously chosen more by empirical approaches and *trials and errors,* are obtained to optimize the synthesis of surfactant-free Pt NPs in alkaline ethylene glycol and to improve reproducibility. *In situ* beam-induced synthesis studied by XANES using H_2PtCl_6 as Pt precursor confirm a reduction mechanism from Pt^{IV} to Pt^{II} and then to Pt^0. NaOH/Pt ratios larger than 2.25 are required to obtain colloidal dispersions in a reproducible way. At high NaOH/Pt molar ratios of 10–20, a fine size control around or even below 1.0 nm is obtained. The results suggest that even higher NaOH/Pt molar ratios will not bring any benefit to the synthesis. This finding is related to slower NP formation kinetics.

On a practical note, with the increasing interest in modelling and machine learning to achieve materials by design, large set of data will be needed to feed algorithms [46]. It is shown here that the surfactant-free polyol synthesis is an ideal model synthesis to acquire such information for Pt; and also for other metals like Ir or Ru [31,45,47]. On a fundamental note, the results indicate different particle formation kinetics for different NaOH/Pt molar ratios, e.g. 10 or 20. However, the resulting particle size is the same. This finding is linked to the known surface functionalization of the NP with OH– and CO_{ad} groups formed from the solvent oxidation. However, the results call for further characterization at the molecular level, to understand further in details the mechanism of nucleation and growth of surfactant-free nanomaterials.

CRediT authorship contribution statement

J. Quinson: Conceptualization, Formal analysis, Funding acquisition, Investigation, Methodology, Visualization, Writing - original draft, Writing - review & editing. **A. Dworzak:** Formal analysis, Investigation, Methodology, Writing - original draft, Writing - review & editing. **S.B. Simonsen:** Resources, Writing - review & editing. **L. Theil Kuhn:** Resources, Writing - review & editing. **K.M.Ø. Jensen:** Funding acquisition, Resources, Supervision, Writing - review & editing. **A. Zana:** Investigation, Writing - review & editing. **M. Oezaslan:** Investigation, Resources, Supervision, Writing - review & editing. **J.J.K. Kirkensgaard:** Resources, Supervision, Writing - review & editing. **M. Arenz:**

Funding acquisition, Investigation, Resources, Supervision, Writing - review & editing.

Declaration of Competing Interest

The authors declare that they have no known competing financial interests or personal relationships that could have appeared to influence the work reported in this paper.

Acknowledgments

This work was funded by the Swiss National Science Foundation (SNSF) via the project No. 200021_184742 (M.A.). J.Q. has received funding from the European Union's Horizon 2020 research and innovation programme under the Marie Skłodowska-Curie grant agreement No 840523 (CoSolCat). K.M.Ø.J. is grateful to the Villum foundation for financial support through a VillumYoung Investigator grant (No. 0015416). J.Q. and J.J.K.K. acknowledge local support and continued access to the University of Copenhagen SAXSLab facility, in particular Martin Schmiele. A. D. and M. O. acknowledge financial support from DFG and BMBF (FOR 2213 and FKZ 03SF0539). The Swiss Light Source (SLS) at the Paul Scherrer Institute, Switzerland is thanked - in particular Dr Maarten Nachtegaal and Dr Olga Safonava - for access to synchrotron beamline SuperXAS (proposal 20161303). F. Bizzotto, V. Mints, J. Schröder are thanked for their help on XAS data acquisition.

Appendix A. Supplementary data

Supplementary data to this article can be found online at https://doi.org/10.1016/j.apsusc.2021.149263.

References

[1] K. An, G.A. Somorjai, Size and shape control of metal nanoparticles for reaction selectivity in catalysis, ChemCatChem 4 (10) (2012) 1512–1524, https://doi.org/10.1002/cctc.201200229.
[2] M. Cargnello, Colloidal nanocrystals as building blocks for well-defined heterogeneous catalysts, Chem. Mater. 31 (3) (2019) 576–596, https://doi.org/10.1021/acs.chemmater.8b04533.
[3] J. Quinson, K.M.Ø. Jensen, From platinum atoms in molecules to colloidal nanoparticles: a review on reduction, nucleation and growth mechanisms, Adv. Colloid Interface Sci. 286 (2020) 102300, https://doi.org/10.1016/j.cis.2020.102300.
[4] F. Fievet, S. Ammar-Merah, R. Brayner, F. Chau, M. Giraud, F. Mammeri, J. Peron, J.-Y. Piquemal, L. Sicarda, G. Viaub, The polyol process: a unique method for easy access to metal nanoparticles with tailored sizes, shapes and compositions, Chem. Soc. Rev. 47 (2018) 5187–5233, https://doi.org/10.1039/C7CS00777A.
[5] D.S. Zhang, B. Goekce, S. Barcikowski, Laser synthesis and processing of colloids: fundamentals and applications, Chem. Rev. 117 (5) (2017) 3990–4103, https://doi.org/10.1021/acs.chemrev.6b00468.
[6] L. Kacenauskaite, J. Quinson, H. Schultz, J.J.K. Kirkensgaard, S. Kunz, T. Vosch, M. Arenz, UV-Induced synthesis and stabilization of surfactant-free colloidal Pt nanoparticles with controlled particle size in ethylene glycol, ChemNanoMat 3 (2) (2017) 89–93, https://doi.org/10.1002/cnma.201600313.
[7] J. Quinson, L. Kacenauskaite, J. Bucher, S.B. Simonsen, L.T. Kuhn, M. Oezaslan, S. Kunz, M. Arenz, Controlled synthesis of surfactant-free water-dispersible colloidal platinum nanoparticles by the Co4Cat process, ChemSusChem 12 (6) (2019) 1229–1239, https://doi.org/10.1002/cssc.201802897.
[8] K.M.O. Jensen, M. Christensen, P. Juhas, C. Tyrsted, E.D. Bojesen, N. Lock, S.J. L. Billinge, B.B. Iversen, Revealing the mechanisms behind SnO_2 nanoparticle formation and growth during hydrothermal synthesis: an in situ total scattering study, J. Am. Chem. Soc. 134 (15) (2012) 6785–6792, https://doi.org/10.1021/ja300978f.
[9] M. Inaba, J. Quinson, J.R. Bucher, M. Arenz, On the preparation and testing of fuel cell catalysts using the thin film rotating disk electrode method, J. Vis. Exp. (2018) e57105, https://doi.org/10.3791/57105.
[10] J. Polte, Fundamental growth principles of colloidal metal nanoparticles - a new perspective, CrystEngComm 17 (36) (2015) 6809–6830, https://doi.org/10.1039/C5CE01014D.
[11] G.J. Hutchings, J.C. Védrine, Heterogeneous Catalyst Preparation, in: M. Baerns (Ed.) Basic Principles in Applied Catalysis. Springer Series in Chemical Physics, vol. 75. Springer, Berlin, Heidelberg, 2004, DOI. 10.1007/978-3-662-05981-4_6.
[12] Z.W. Seh, J. Kibsgaard, C.F. Dickens, I.B. Chorkendorff, J.K. Norskov, T. F. Jaramillo, Combining theory and experiment in electrocatalysis: insights into materials design, Science 355 (6321) (2017), https://doi.org/10.1126/science.aad4998.
[13] J. Boita, L. Nicolao, M.C.M. Alves, J. Morais, Observing Pt nanoparticle formation at the atomic level during polyol synthesis, Phys. Chem. Chem. Phys. 16 (33) (2014) 17640–17647, https://doi.org/10.1039/C4CP01925C.
[14] S.M. Chen, Q.Y. Yang, H.H. Wang, S. Zhang, J. Li, Y. Wang, W.S. Chu, Q. Ye, L. Song, Initial reaction mechanism of platinum nanoparticle in methanol-water system and the anomalous catalytic effect of water, Nano Lett. 15 (9) (2015) 5961–5968, https://doi.org/10.1021/acs.nanolett.5b02098.
[15] M. Harada, Y. Kamigaito, Nucleation and aggregative growth process of platinum nanoparticles studied by in situ quick XAFS spectroscopy, Langmuir 28 (5) (2012) 2415–2428, https://doi.org/10.1021/la204031j.
[16] B. Abecassis, F. Testard, O. Spalla, P. Barboux, Probing in situ the nucleation and growth of gold nanoparticles by small-angle x-ray scattering, Nano Lett. 7 (6) (2007) 1723–1727, https://doi.org/10.1021/nl0707149.
[17] J. Quinson, J.K. Mathiesen, J. Schroder, A. Dworzak, F. Bizzotto, A. Zana, S. B. Simonsen, L. Theil Kuhn, M. Oezaslan, K.M.Ø. Jensen, M. Arenz, Teaching old precursors new tricks: fast room temperature synthesis of surfactant-free colloidal platinum nanoparticles, J. Colloid Interface Sci. 577 (2020) 319–328, https://doi.org/10.1016/j.jcis.2020.05.078.
[18] V.K. LaMer, R.H. Dinegar, Theory, production and mechanism of formation of monodispersed hydrosols, J. Am. Chem. Soc. 72 (11) (1950) 4847–4854, https://doi.org/10.1021/ja01167a001.
[19] M. Harada, N. Tamura, M. Takenaka, Nucleation and growth of metal nanoparticles during photoreduction using in situ time-resolved SAXS analysis, J. Phys. Chem. C 115 (29) (2011) 14081–14092, https://doi.org/10.1021/jp203119a.
[20] H. Zheng, R.K. Smith, Y.-W. Jun, C. Kisielowski, U. Dahmen, A.P. Alivisatos, Observation of single colloidal platinum nanocrystal growth trajectories, Science 324 (5932) (2009) 1309–1312, https://doi.org/10.1126/science.1172104.
[21] S. Cheong, J. Watt, B. Ingham, M.F. Toney, R.D. Tilley, In situ and ex situ studies of platinum nanocrystals: growth and evolution in solution, J. Am. Chem. Soc. 131 (40) (2009) 14590–14595, https://doi.org/10.1021/ja9065688.
[22] J. Quinson, S. Neumann, T. Wannmacher, L. Kacenauskaite, M. Inaba, J. Bucher, F. Bizzotto, S.B. Simonsen, L.T. Kuhn, D. Bujak, A. Zana, M. Arenz, S. Kunz, Colloids for catalysts: a concept for the preparation of superior catalysts of industrial relevance, Ang. Chem. Int. Ed. 57 (38) (2018) 12338–12341, https://doi.org/10.1002/anie.201807450.
[23] L.L. Fan, X.X. Du, Z.X. Kang, H.L. Guo, W.P. Kang, M. Xue, D.F. Sun, N-doped hollow carbon nanospheres as platinum anchoring material for efficient hydrogen evolution, Appl. Surf. Sci. 459 (2018) 453–458, https://doi.org/10.1016/j.apsusc.2018.08.033.
[24] E. Bertin, A. Munzer, S. Reichenberger, R. Streubel, T. Vinnay, H. Wiggers, C. Schulz, S. Barcikowski, G. Marzun, Durability study of platinum nanoparticles supported on gas-phase synthesized graphene in oxygen reduction reaction conditions, Appl. Surf. Sci. 467 (2019) 1181–1186, https://doi.org/10.1016/j.apsusc.2018.10.061.
[25] M.V. Kovalenko, L. Manna, A. Cabot, Z. Hens, D.V. Talapin, C.R. Kagan, V. I. Klimov, A.L. Rogach, P. Reiss, D.J. Milliron, P. Guyot-Sionnnest, G. Konstantatos, W.J. Parak, T. Hyeon, B.A. Korgel, C.B. Murray, W. Heiss, Prospects of nanoscience with nanocrystals, ACS Nano 9 (2) (2015) 1012–1057, https://doi.org/10.1021/nn506223h.
[26] A. Tata, B. Gralec, E. Proniewicz, Unsupported platinum nanoparticles as effective sensors of neurotransmitters and possible drug curriers, Appl. Surf. Sci. 435 (2018) 256–264, https://doi.org/10.1016/j.apsusc.2017.11.100.
[27] E. Antolini, Structural parameters of supported fuel cell catalysts: the effect of particle size, inter-particle distance and metal loading on catalytic activity and fuel cell performance, Appl. Catal. B 181 (2016) 298–313, https://doi.org/10.1016/j.apcatb.2015.08.007.
[28] K.M. Koczkur, S. Mourdikoudis, L. Polavarapu, S.E. Skrabalak, Polyvinylpyrrolidone (PVP) in nanoparticle synthesis, Dalton Trans. 44 (41) (2015) 17883–17905, https://doi.org/10.1039/C5DT02964C.
[29] M. Cargnello, C. Chen, B.T. Diroll, V.V.T. Doan-Nguyen, R.J. Gorte, C.B. Murray, Efficient removal of organic ligands from supported nanocrystals by fast thermal annealing enables catalytic studies on well-defined active phases, J. Am. Chem. Soc. 137 (21) (2015) 6906–6911, https://doi.org/10.1021/jacs.5b03333.
[30] D.G. Li, C. Wang, D. Tripkovic, S.H. Sun, N.M. Markovic, V.R. Stamenkovic, Surfactant removal for colloidal nanoparticles from solution synthesis: the effect on catalytic performance, ACS Catal. 2 (7) (2012) 1358–1362, https://doi.org/10.1021/cs300219j.
[31] Y. Wang, J.W. Ren, K. Deng, L.L. Gui, Y.Q. Tang, Preparation of tractable platinum, rhodium, and ruthenium nanoclusters with small particle size in organic media, Chem. Mater. 12 (6) (2000) 1622–1627, https://doi.org/10.1021/cm0000853.
[32] S. Neumann, J. Schroder, F. Bizzotto, M. Arenz, A. Dworzak, M. Oezaslan, M. Baumer, S. Kunz, Halide-induced leaching of Pt nanoparticles - manipulation of particle size by controlled Ostwald ripening, ChemNanoMat 5 (4) (2019) 462–471, https://doi.org/10.1002/cnma.201800550.
[33] I. Schrader, J. Warneke, S. Neumann, S. Grotheer, A.A. Swane, J.J.K. Kirkensgaard, M. Arenz, S. Kunz, Surface chemistry of "unprotected" nanoparticles: a Spectroscopic investigation on colloidal particles, J. Phys. Chem. C 119 (31) (2015) 17655–17661, https://doi.org/10.1021/acs.jpcc.5b03863.
[34] C. Bock, C. Paquet, M. Couillard, G.A. Botton, B.R. MacDougall, Size-selected synthesis of PtRu nano-catalysts: reaction and size control mechanism, J. Am. Chem. Soc. 126 (25) (2004) 8028–8037, https://doi.org/10.1021/ja0495819.
[35] J. Quinson, M. Inaba, S. Neumann, A.A. Swane, J. Bucher, S.B. Simonsen, L. T. Kuhn, J.J.K. Kirkensgaard, K.M.O. Jensen, M. Oezaslan, S. Kunz, M. Arenz, Investigating particle size effects in catalysis by applying a size-controlled and surfactant-free synthesis of colloidal nanoparticles in alkaline ethylene glycol: case

study of the oxygen reduction reaction on Pt, ACS Catal. 8 (7) (2018) 6627–6635, https://doi.org/10.1021/acscatal.8b00694.
[36] M. Newville, IFEFFIT: interactive XAFS analysis and FEFF fitting, J. Synchrotron Radiat. 8 (2001) 322–324, https://doi.org/10.1107/S0909049500016964.
[37] T. Li, A.J. Senesi, B. Lee, Small angle X-ray scattering for nanoparticle research, Chem. Rev. 116 (18) (2016) 11128–11180, https://doi.org/10.1021/acs.chemrev.5b00690.
[38] J. Quinson, S. Neumann, L. Kacenauskaite, J. Bucher, J.J.K. Kirkensgaard, S. B. Simonsen, L. Theil Kuhn, A. Zana, T. Vosch, M. Oezaslan, S. Kunz, M. Arenz, Solvent-dependent growth and stabilization mechanisms of surfactant-free colloidal Pt nanoparticles, Chem. Eur. J. 26 (41) (2020) 9012–9023.
[39] N. Steinfeldt, In situ monitoring of Pt nanoparticle formation in ethylene glycol solution by SAXS-influence of the NaOH to Pt Ratio, Langmuir 28 (36) (2012) 13072–13079, https://doi.org/10.1021/la3026232.
[40] T. Yao, S.J. Liu, Z.H. Sun, Y.Y. Li, S. He, H. Cheng, Y. Xie, Q.H. Liu, Y. Jiang, Z. Y. Wu, Z.Y. Pan, W.S. Yan, S.Q. Wei, Probing nucleation pathways for morphological manipulation of platinum nanocrystals, J. Am. Chem. Soc. 134 (2012) 9410–9416, https://doi.org/10.1021/ja302642x.
[41] N.T.K. Thanh, N. Maclean, S. Mahiddine, Mechanisms of nucleation and growth of nanoparticles in solution, Chem. Rev. 114 (15) (2014) 7610–7630, https://doi.org/10.1021/cr400544s.
[42] D.R. Handwerk, P.D. Shipman, C.B. Whitehead, S. Ozkar, R.G. Finke, Mechanism-enabled population balance modeling of particle formation en route to particle average size and size distribution understanding and control, J. Am. Chem. Soc. 141 (40) (2019) 15827–15839, https://doi.org/10.1021/jacs.9b06364.
[43] S. Mozaffari, W.H. Li, C. Thompson, S. Ivanov, S. Seifert, B. Lee, L. Kovarik, A. M. Karim, Colloidal nanoparticle size control: experimental and kinetic modeling investigation of the ligand metal binding role in controlling the nucleation and growth kinetics, Nanoscale 9 (36) (2017) 13772–13785, https://doi.org/10.1039/C7NR04101B.
[44] B.J. Hwang, L.S. Sarma, C.H. Chen, C. Bock, F.J. Lai, S.H. Chang, S.C. Yen, D.G. Liu, H.S. Sheu, J.F. Lee, Controlled synthesis and characterization of Ru-core-Pt-shell bimetallic nanoparticles, J. Phys. Chem. C 112 (50) (2008) 19922–19929, https://doi.org/10.1021/jp807154a.
[45] S. Neumann, S. Grotheer, J. Tielke, I. Schrader, J. Quinson, A. Zana, M. Oezaslan, M. Arenz, S. Kunz, Nanoparticles in a box: a concept to isolate, store and re-use colloidal surfactant-free precious metal nanoparticles, J. Mater. Chem. A 5 (13) (2017) 6140–6145, https://doi.org/10.1039/C7TA00628D.
[46] B.G. Sumpter, R.K. Vasudevan, T. Potok, S.V. Kalinin, A bridge for accelerating materials by design, Npj Comput. Mater. 1 (2015), https://doi.org/10.1038/npjcompumats.2015.8.
[47] J.A. Arminio-Ravelo, J. Quinson, M.A. Pedersen, J.J.K. Kirkensgaard, M. Arenz, M. Escudero-Escribano, Synthesis of iridium nanocatalysts for water oxidation in acid: effect of the surfactant, ChemCatChem 12 (5) (2020) 1282–1287, https://doi.org/10.1002/cctc.201902190.